frontiers | Frontiers in Materials

ORIGINAL RESEARCH
published: 20 May 2022
doi: 10.3389/fmats.2022.907672

Reconfigurable Metasurface Hologram of Dynamic Distance *via* Deep Learning

Yijun Zou[1,2], *Rongrong Zhu*[1,2]*, *Lian Shen*[1] and *Bin Zheng*[1,3,4]*

[1]Interdisciplinary Center for Quantum Information, State Key Laboratory of Modern Optical Instrumentation, ZJU-Hangzhou Global Scientic and Technological Innovation Center, Zhejiang University, Hangzhou, China, [2]School of Information and Electrical Engineering, Zhejiang University City College, Zhejiang, China, [3]International Joint Innovation Center, Key Laboratory of Advanced Micro/Nano Electronic Devices and Smart Systems of Zhejiang, The Electromagnetics Academy at Zhejiang University, Zhejiang University, Haining, China, [4]Jinhua Institute of Zhejiang University, Zhejiang University, Jinhua, China

Reconfigurable metasurfaces have been regarded as an emerging subfield of metasurfaces that can manipulate electromagnetic wave information in a smart manner. They stimulate a gradual transition in metasurface holography from passive to active elements. To date, intelligent dynamic holographic imaging schemes typically rely on iterative or data-driven methods to obtain holograms at a fixed imaging distance, which significantly hinders the development of intelligent dynamic holographic imaging in practical scenarios involving high demands for dynamic imaging distances. Herein, a computer-generated hologram algorithm with a dynamic imaging distance and a reconfigurable metasurface are proposed, which is referred to as a generator and physical diffractive network. Simulation results of time–distance division for three-dimensional imaging are provided to demonstrate the reliability and high efficiency of the proposed algorithm.

Keywords: metasurfaces, holography, imaging, deep learning, diffractive model

OPEN ACCESS

Edited by:
Chen Shen,
Rowan University, United States

Reviewed by:
Yuxin Zhai,
University of Michigan, United States
Si Jia Li,
Southeast University, China

***Correspondence:**
Rongrong Zhu
rorozhu@zju.edu.cn
Bin Zheng
zhengbin@zju.edu.cn

Specialty section:
This article was submitted to Metamaterials, a section of the journal Frontiers in Materials

Received: *30 March 2022*
Accepted: *20 April 2022*
Published: *20 May 2022*

Citation:
Zou Y, Zhu R, Shen L and Zheng B (2022) Reconfigurable Metasurface Hologram of Dynamic Distance via Deep Learning. Front. Mater. 9:907672. doi: 10.3389/fmats.2022.907672

INTRODUCTION

Holography is one of the most promising three-dimensional (3D) imaging techniques that can integrally reconstruct an imaging target by recording the amplitude and phase information of electromagnetic wavefronts(Gabor, 1948) (Leith and Upatnieks, 1962). Breakthroughs in computer-generated holograms and spatial light modulators(Xu et al., 2017) have enabled the creation of holograms of virtual objects. Holography have garnered significant attention in the fields of metrology(Kreis et al., 2001; Mundt and Kreis, 2010; Desse and Picart, 2015), data storage (Hesselink et al., 2004) (Kim et al., 2009), and displays (Cem et al., 2020) (Shi et al., 2021). However, several challenges remain to be overcome. Reconstruction using bulky macroscale interference-based generation methods(Tricoles, 1987) has many physical limitations, such as narrow bandwidths, small fields of view, and multiple diffraction orders.

The emergence of metamaterials(Huang and Chen, 2011) (Chen et al., 2004) in recent years has provided novel perspectives for the modulation of light and electromagnetic waves. Metamaterials have generated tremendous attention in the field of cloak(Chen et al., 2007; Xi et al., 2009; Xu et al., 2012) etc. Metasurfaces(Allen et al., 2020; Han et al., 2021; Hu et al., 2021; Yang et al., 2016; Pfeiffer and Grbic, 2013) are ultrathin subwavelength planar metamaterials that can control electromagnetic wavefronts into almost arbitrary profiles. Metasurfaces have become an excellent solution for

holograms owing to their ability to control electromagnetic waves(Wang et al., 2016a; Devlin et al., 2016; Zhang et al., 2016; Yan et al., 2021). Compared with conventional holograms, metasurface-based holograms provide unprecedented spatial resolution, high precision and low noise. The subwavelength pixel-sized unit can contribute to excellent holographic imaging owing to the elimination of undesired diffraction orders and improvements in the transmission or reflection efficiency.

Recently, reconfigurable metasurfaces(Li et al., 2020; Li et al., 2021; Wu et al., 2021; Li et al., 2022) have been proposed to realise various functionalities by integrating them with phase-changing materials. Reconfigurable metasurfaces have been used to implement holograms for dynamic control. For instance, coding metasurface holograms can be generated using a 1-bit Gerchberg-Saxton algorithm(Li et al., 2017) or a dichotomous neural network (Liu et al., 2021) (Liu et al., 2022). The iterative-based GS algorithm must satisfy the Fourier correspondence between forward and backward diffractions, which exists only in the far field. In terms of the dynamic imaging distance, an overly large solution space and phase periodicity results in a network that is difficult to converge. However, a dynamic imaging distance is required when a complex imaging environment is involved.

In this study, a holographic imaging mathematical model was constructed to analyse the inverse design problem, and the phase-generation problem of the generator and physical diffractive network (GPDN) was resolved using a two-channel method. Specifically, the structure of the GPDN was combined with a physical diffraction model to facilitate the unsupervised training of the network, including the metasurface and diffraction layers. The proposed method can rapidly generate a hologram when the target and distance are specified. A reconfigurable metasurface for 3D imaging at approximately 6 GHz was designed to validate the proposed method. Specifically, the 3D model was partitioned into imaging targets and distances at equal spacings, which generated 20 × 20 supercell holograms in real time, and the simulation results validated the efficiency and reliability of this approach.

THEORY AND METHOD

Figure 1 shows a schematic illustration of the proposed dynamic-distance holographic imaging system. The holograms are generated after inputting the image and distance of the 3D model slice to the generator of GPDN; subsequently, the reconfigurable metasurfaces yield the corresponding holograms via a voltage control module.

The Rayleigh–Sommerfeld diffraction formula (Wang et al., 2016b). is acknowledged as a forward propagation function from the phase distribution of metasurfaces to the near-field EM distribution.

$$U(r_1) = \iint_{\Sigma} U(r_0) \frac{1}{i\lambda} \cos < n, r_{10} > \frac{\exp(-ikr_{10})}{r_{10}} ds \tag{1}$$

where $U(r_0)$ and $U(r_1)$ represent the electric fields at point R_0 on the metasurface and at point R_1 on the imaging plane, respectively; λ is the wavelength in air; r_{01} is the distance between R_0 and R_1; $\cos < n, r_{01} >$ is the inclination factor. In the near field, it can be expressed in a simpler form as follows:

$$U(r_1) = \frac{\mathrm{d}}{i\lambda} \iint_{\Sigma} U(r_0) \frac{\exp(-ikr_{10})}{r_{10}^2} ds \tag{2}$$

In a two-dimensional (2D) imaging system, this expression can be decomposed into a mathematical convolution, as follows:

$$U(r_1) = \frac{\mathrm{d}}{i\lambda} U(r_0) * \frac{\exp(-ikr_0)}{r_0^2} | r_0 = r_1 \tag{3}$$

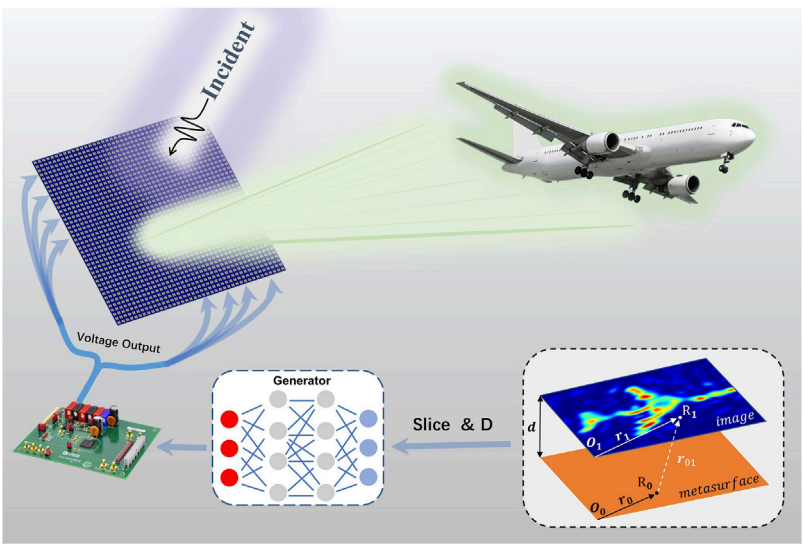

FIGURE 1 | Schematic illustration of holographic imaging system.

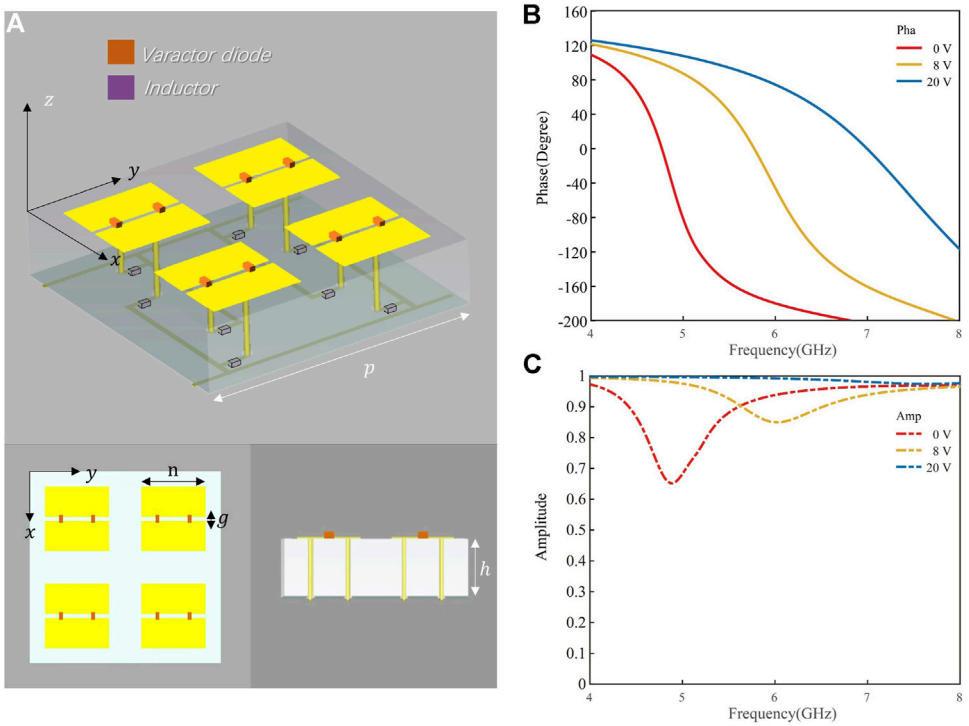

FIGURE 2 | (A) Structure of supercell **(B)** phase responses of supercell at 0, 8, and 20 V **(C)** amplitude responses of supercell at 0, 8, and 20 V.

This formula can be calculated via the Fourier transform to reduce the computational complexity, as follows:

$$U(r_1) = \frac{\mathrm{d}}{i\lambda} F^{-1}\left(F(U(r_0)) * F\left(\frac{\exp(-ikr_0)}{r_0^2} \right) \right) | r_0 = r_1 \quad (4)$$

The effect of each pixel on the imaging is the same at a fixed imaging distance; however, the phase periodicity of each pixel causes multi-solution uncertainty. In other words, the imaging result is the same for a phase hologram and the initial phase. Furthermore, the addition of a dynamic imaging distance directly results in network convergence failure.

To suppress the corner-related scattering effect (Li et al., 2017). of reconfigurable metasurface units, 2 × 2 reconfigurable metasurface units were arranged in a supercell. In each reconfigurable metasurface unit, two planar symmetrical metallic sheets were printed on the top surface of the substrate, and two varactor diodes were loaded between them; the substrate had a dielectric constant of 3.5. For each planar structure, two metallic via holes were drilled through the substrate to connect the top structure, and they were independent of the ground to provide a direct current (DC) bias voltage. Hence, each supercell can independently realise the required phase by controlling the voltage bias. The total size of the supercell is $p*p*h$ ($p = 30mm$, $h = 3mm$). Four identical sub-cells together make up the supercell. On the top surface of sub-cell, two planar metal structures of length $n = 10mm$ are printed out $g = 0.6mm$ apart. They are connected by two varactor diodes(SMV-2019 (Zhang et al., 2013)). Two metallic via holes are drilled to input the biased direct current (DC) voltages. The 1 nH inductors connect to the vias to reduce the influence of the feed line on the electromagnetic response of the unit cell (**Figure 2A**). At x-polarization incident wave and DC bias of 0–20 V, the supercell can provide phase variations from -180° to 100° (**Figure 2B**) and a reflectivity minimum of 0.85 at 6 GHz (**Figure 2C**).

Figure 3 shows the structure of the proposed GPDN. It comprises two main modules: a generator and a physical diffraction model. The generator uses a special multi-layer perceptron (MLP) model. In particular, the 40*40 image is stretched and stiches with the distance to form the 1601*1 vector for input of the MLP. The input layer generates dual channel vector in the first hidden layer via two parallel independent weights and biases. The second hidden layer and output layer work similarly to the above. Finally, the 400*2 feature vector characterizing the real and imaginary parts is captured and then synthesizes the phase parameters ranging from →π to π via Atan2 function. This approach allows the generator of GPDN to uniquely output any phase, which can avoid network oscillation owing to the periodicity of the phase. The physical diffractive model comprises two layers: a metasurface layer and a diffractive layer. The metasurface layer synthesises phase parameters based on the phase response with the ground performance of the supercell, which is further compressed to -180° to 100°, and the amplitude varies with phase. This network structure of

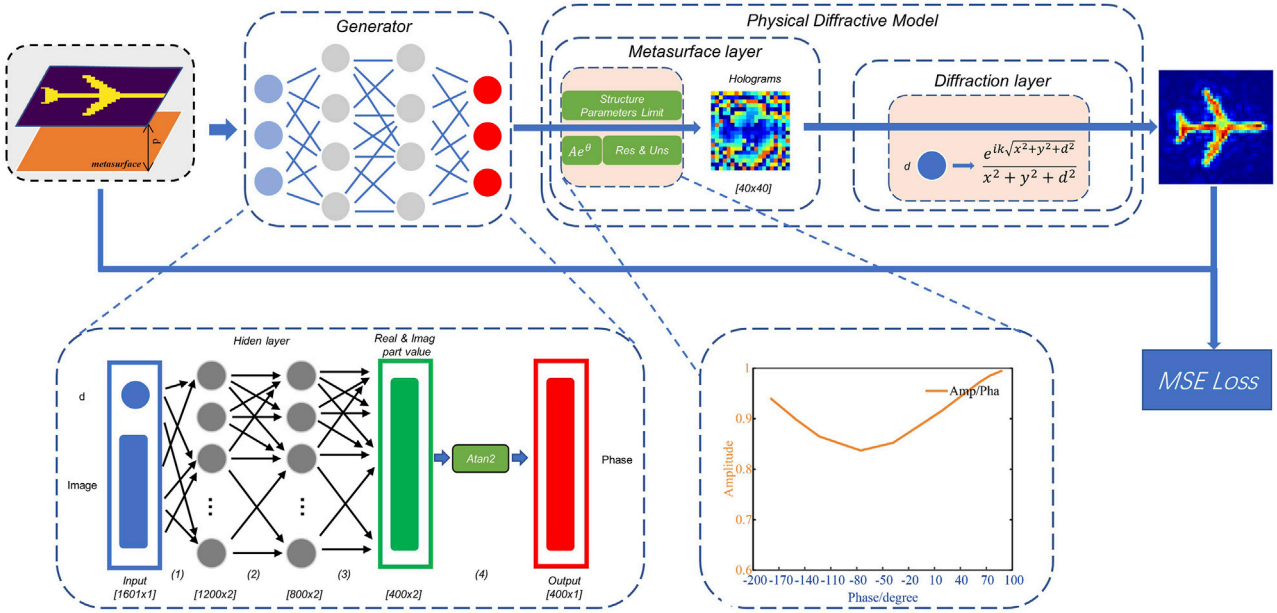

FIGURE 3 | Structure of GPDN, which comprises two modules: generator and physical diffractive model. Physical diffraction model includes metasurface and diffraction layers.

GPDN solves the physical limitations of reconfigurable metasurface units. Our GPDN can be used by re-measuring the phase compression relationship and amplitude–phase change curve for any new reconfigurable metasurface unit. Subsequently, the metasurface layer generates a 40 × 40 metasurface hologram via reshaping and unsampling functions, and every four adjacent pixels share the same phase value corresponding to a supercell. Subsequently, holographic imaging results are generated by the diffractive layer and divided by its maximum value to maintain its value in the range [0,1] to facilitate comparison with the imaging target. It is noteworthy that each diffractive matrix is determined by the imaging distance, and to ensure the rigor of the diffraction computation, other parameters in the diffraction matrix are not updated in the backward propagation. The diffraction layer renders it to avoid construct a label for supervised training and directly obtains the imaging results at the corresponding imaging distance; the diffraction layer also allows the special solution channels at each imaging distance to be retained to alleviate the severe multi-solution problem caused by the large solution space.

The mean square error (MSE) is calculated as an index to measure the similarity between the reconstructed and target images; it facilitates the GPDN in completing gradient backward propagation.

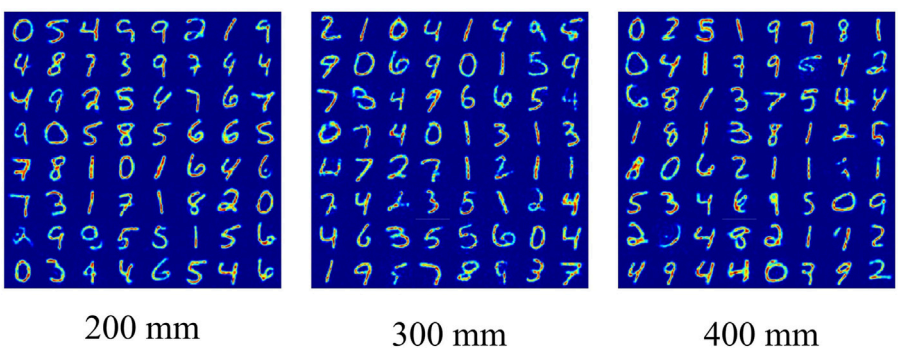

FIGURE 4 | Imaging results of hologram obtained via numerical simulation based on generator inputs of d = 200, 300, and 400 mm.

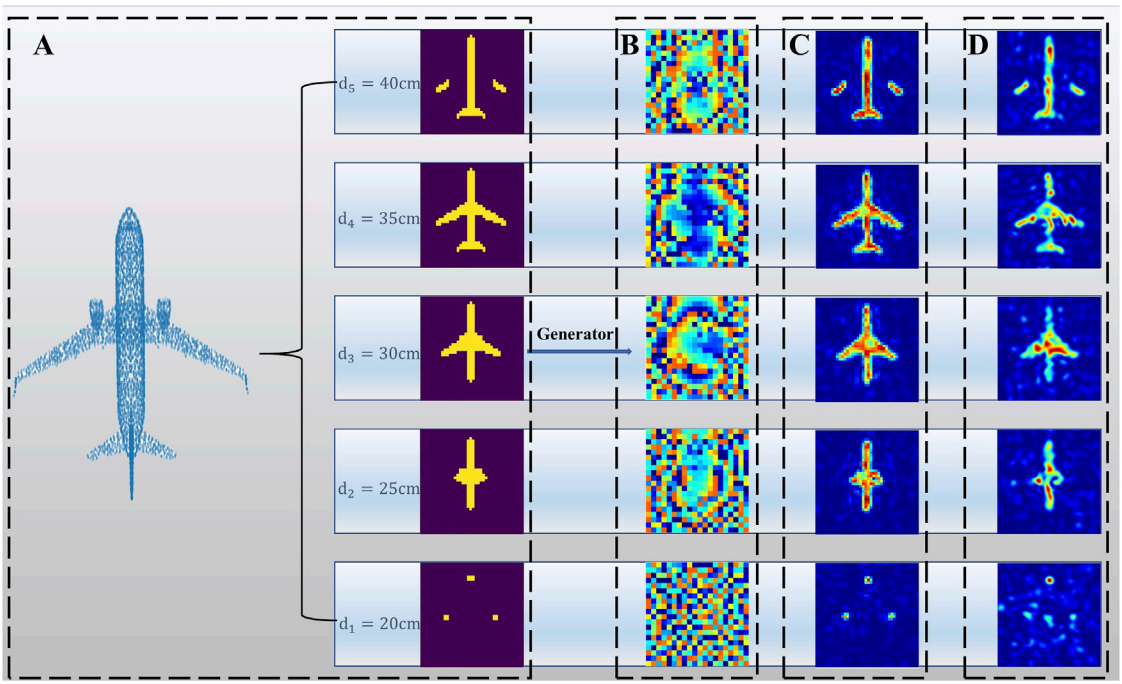

FIGURE 5 | (A) Three-dimensional airplane model segregated into two-dimensional Images at five different distances **(B)** Holograms yielded by generator based on images and distances **(C)** Diffraction imaging results obtained via numerical simulation at corresponding distance **(D)** Full-wave simulation results based on supercell obtained *via* CST.

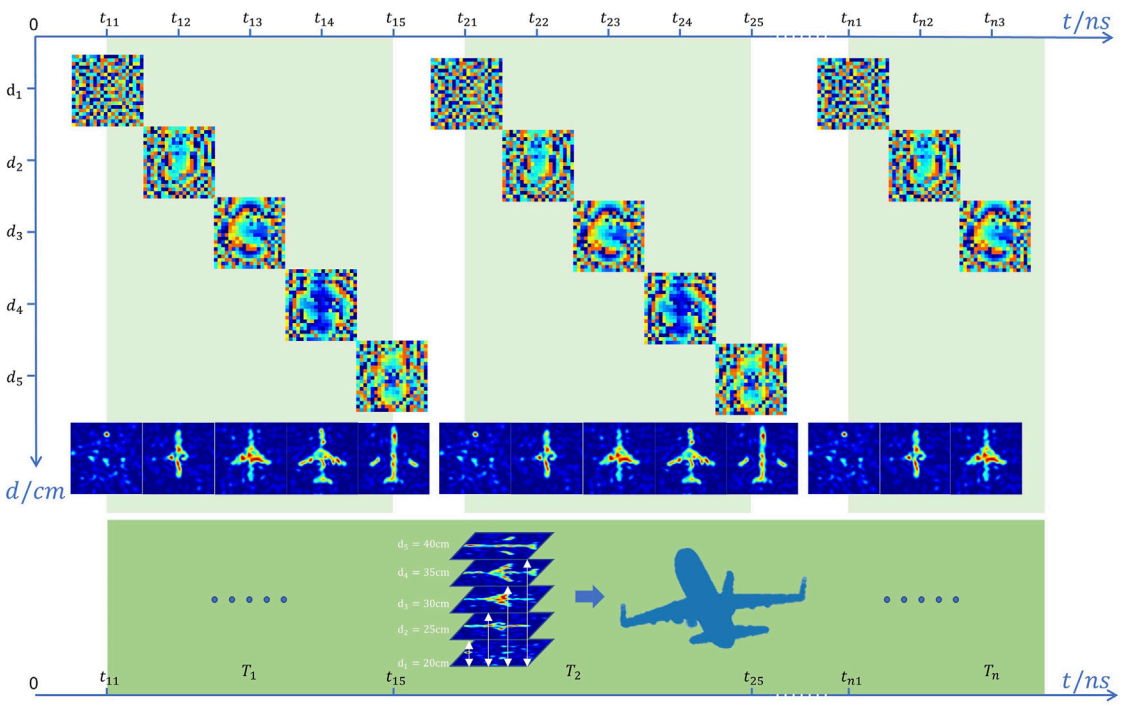

FIGURE 6 | Time–distance division of 3D imaging system.

$$MSE = \frac{1}{N}\sum\left[\left(E_{out} - E_{\text{target}}\right)^2\right] \tag{5–1}$$

$$\frac{\partial MSE}{\partial E} = \frac{2}{N}\left[\left(E_{out} - E_{\text{target}}\right)\right]^T \tag{5–2}$$

RESULTS AND DISCUSSIONS

Approximately 60,000 data points including imaging distances of 200–400 mm and random imaging targets were generated, and they supported the unsupervised training of the GPDN. The Adam optimiser was set at a learning rate of 1e-3, and the batch size was 64. A program was developed using a PyTorch deep-learning platform on a GPU (1050Ti). After approximately 1000 epochs, the *MSE* loss stabilised. We selected imaging distances of 200, 300, and 400 mm, as well as random handwritten digit targets from the MNIST dataset as inputs to generate 64 holograms for each distance. To ensure the rigor of the reconstruction results, holographic imaging corresponding to imaging distances was numerically generated using the diffraction formula. **Figure 4** shows the imaging results, which indirectly illustrate the effectiveness of the hologram and the interpretability of the GPDN's physical diffraction model.

For 3D holographic imaging, an increase in the spatial dimension implies more meta units required to restore the information. Currently, partitioning a 3D target into a 2D target and the distance to reduce the complexity of the imaging system is a smart scheme. An airplane model can be segmented into slices every 5 cm along the Z-axis. The slices and corresponding imaging distances are shown in **Figure 5A**, which can be used to generate the target holograms by the generator, as shown in **Figure 5B**. **Figure 5C** shows the imaging numerical simulation results generated using the exact diffraction formula. To verify the effectiveness of the proposed GPDN model based on physics, we used the commercial software CST STUDIO SUITE to perform a full-wave simulation (**Figure 5D**), and the supercell structure was as described above. In particular, the results of the full-wave and numerical simulations were highly consistent, which is attributable to two reason. First, the metasurface and diffractive layers provide many physical constraints to the hologram, which renders the holographic imaging system similar to the practical scenario. Second, the phase holograms generated by any network are considered messy, which may destroy the periodicity of the metasurfaces and result in unit coupling. Therefore, a supercell was used in this system. Moreover, excellent performance was no longer required in the optical response of the metasurface unit, such as 2π phase coverage or amplitude uniformity. Consequently, the abovementioned GPDN structure is applicable to other imaging problems and hence can reduce difficulties in complex imaging systems.

The holographic display of the 3D model can be realised using time–distance division technology. However, the cost is expressed in the time domain. Nonetheless, the reconfigurable metasurface unit can expand the time dimension. Each subholographic image can be completed by a one-time adjustment of the phase distribution, i.e. holographic imaging is not completely generated until metasurfaces traverse the phase distributions corresponding to all imaging distance points. Based on the datasheet of the varactor diode (SMV-2019), its response speed is 10ns. The DAC (AD5535) requires 32 communication instructions to control the output voltage, and the baud rate is 115200, which corresponds to 270μs. Thirteen DACs were used in this study. Therefore, approximately 3.6ms was required to change the phase distribution of the metasurfaces at a time. The metasurfaces achieved a stable electric field distribution with 3.6ms. Regarding the time of five-phase reconstruction as a period T, which was 18ms, the same sub-image appeared once every 18ms, as shown in **Figure 6**. In a continuous and stable periodic cycle, it appears as a complete holographic 3D image and has been fully implemented for high-quality imaging.

CONCLUSION

In this study, a reconfigurable metasurface holographic imaging system with adjustable distance was designed. In particular, we innovatively added a metasurface layer to the system, which allows the output of the hologram to be adjusted according to the optical response of the unit, thereby rendering the entire physical diffractive model more accurate. Consequently, the imaging system can rapidly regulate the state of the reconfigurable metasurface elements to control the distribution of near-field electromagnetic waves and display 3D holographic images. In addition, the proposed method can be easily extended to dynamic frequencies. We believe that a more comprehensive imaging system will be developed in the near future.

DATA AVAILABILITY STATEMENT

The raw data supporting the conclusion of this article will be made available by the authors, without undue reservation.

AUTHOR CONTRIBUTIONS

B. Z. and R. Z. conceived the idea and supervised the the research. B. Z. and R. Z. guided the theory. Y. Z. designed the algorithm framework and unit Structure. Y. Z. and L. S. performed the numerical and simulation verifications. Y. Z., B. Z., R. Z. and L. S. analyzed the data. Y. Z. and L. S. wrote the paper. All authors discussed the results and commented on the manuscript.

FUNDING

This work was sponsored by the National Natural Science Foundation of China under Grant Nos. 62071423 and 61905216, Natural Science Foundation of Zhejiang Province under Grant No. LQ21F050002, and Fundamental Research Funds for the Central Universities.

REFERENCES

Allen, K. W., Dykes, D. J. P., Reid, D. R., and Lee, R. T. (2020). Multi-Objective Genetic Algorithm Optimization of Frequency Selective Metasurfaces to Engineer Ku-Passband Filter Responses. *Prog. Electromagn. Res.* 167, 19–30. doi:10.2528/pier19112609

Cem, A., Hedili, M. K., Ulusoy, E., and Urey, H. (2020). Foveated Near-Eye Display Using Computational Holography. *Sci. Rep.* 10, 14905. doi:10.1038/s41598-020-71986-9

Chen, H., Ran, L., Huangfu, J., Zhang, X., Chen, K., Grzegorczyk, T. M., et al. (2004). Left-handed Materials Composed of Only S-Shaped Resonators. *Phys. Rev. E Stat. Nonlin Soft Matter Phys.* 70, 057605. doi:10.1103/PhysRevE.70.057605

Chen, H., Wu, B.-I., Zhang, B., and Kong, J. A. (2007). Erratum: Electromagnetic Wave Interactions with a Metamaterial Cloak [Phys. Rev. Lett.99, 063903 (2007)]. *Phys. Rev. Lett.* 99, 149901. doi:10.1103/physrevlett.99.149901

Desse, J.-M., and Picart, P. (2015). Stochastic Digital Holography for Visualizing inside Strongly Refracting Transparent Objects. *Appl. Opt.* 54, A1–A8. doi:10.1364/ao.54.0000a1

Devlin, R. C., Khorasaninejad, M., Chen, W. T., Oh, J., and Capasso, F. (2016). Broadband High-Efficiency Dielectric Metasurfaces for the Visible Spectrum. *Proc. Natl. Acad. Sci. U.S.A.* 113, 10473–10478. doi:10.1073/pnas.1611740113

Gabor, D. (1948). A New Microscopic Principle. *Nature* 161, 777–778. doi:10.1038/161777a0

Han, B., Li, S., Li, Z., Huang, G., Tian, J., and Cao, X. (2021). Asymmetric Transmission for Dual-Circularly and Linearly Polarized Waves Based on a Chiral Metasurface. *Opt. Express* 29, 19643–19654. doi:10.1364/oe.425787

Hesselink, L., Orlov, S. S., and Bashaw, M. C. (2004). Holographic Data Storage Systems. *Proc. IEEE* 92, 1231–1280. doi:10.1109/jproc.2004.831212

Hu, Z., He, N., Sun, Y., Jin, Y., and He, S. (2021). Wideband High-Reflection Chiral Dielectric Metasurface. *Prog. Electromagn. Res.* 172, 51–60. doi:10.2528/pier21121903

Huang, L., and Chen, H. (2011). Multi-band and Polarization Insensitive Metamaterial Absorber. *Prog. Electromagn. Res.* 113, 103–110. doi:10.2528/pier10122401

Kim, J. H., Yang, H., and Park, J. B. (2009). "IPI Noise Reduction by Fuzzy Rules and Data Compression Using Wavelet Transform Method in a Holographic Data Storage System," in *Optical Data Storage Topical Meeting*, 55–57. doi:10.1109/ods.2009.5031752

Kreis, T. M., Aswendt, P., and Höfling, R. (2001). Hologram Reconstruction Using a Digital Micromirror Device. *Opt. Eng.* 40, 926–933. doi:10.1117/1.1367346

Leith, E. N., and Upatnieks, J. (1962). Reconstructed Wavefronts and Communication Theory*. *J. Opt. Soc. Am.* 52, 1123–1130. doi:10.1364/josa.52.001123

Li, L., Jun Cui, T., Ji, W., Liu, S., Ding, J., Wan, X., et al. (2017). Electromagnetic Reprogrammable Coding-Metasurface Holograms. *Nat. Commun.* 8, 197. doi:10.1038/s41467-017-00164-9

Li, S. J., Li, Y. B., Li, R. Q., Li, Z. X., Zhang, C., Guo, Z. X., et al. (2020). A Thin Self-Feeding Janus Metasurface for Manipulating Incident Waves and Emitting Radiation Waves Simultaneously. *Ann. Der Phys.* 532, 2000020. doi:10.1002/andp.202000020

Li, S. J., Li, Y. B., Zhang, L., Luo, Z. J., Han, B. W., Li, R. Q., et al. (2021). Programmable Controls to Scattering Properties of a Radiation Array. *Laser & Photonics Rev.* 15, 2000449. doi:10.1002/lpor.202000449

Li, S., Li, Z., Han, B., Huang, G., and Liu, X. (2022). Multifunctional Coding Metasurface with Left and Right Circularly Polarized and Multiple Beams. *Front. Mat.* 854062. doi:10.3389/fmats.2022.854062

Liu, C., Yu, W. M., Ma, Q., Li, L., and Cui, T. J. (2021). Intelligent Coding Metasurface Holograms by Physics-Assisted Unsupervised Generative Adversarial Network. *Phot. Res.* 9, B159–B167. doi:10.1364/prj.416287

Liu, C., Ma, Q., Luo, Z. J., Hong, Q. R., Xiao, Q., Zhang, H. C., et al. (2022). A Programmable Diffractive Deep Neural Network Based on a Digital-Coding Metasurface Array. *Nat. Electron.* 5, 113–122. doi:10.1038/s41928-022-00719-9

Mundt, J., and Kreis, T. (2010). Digital Holographic Recording and Reconstruction of Large-Scale Objects for Metrology and Display. *Opt. Eng.* 49, 125801. doi:10.1117/1.3524238

Pfeiffer, C., and Grbic, A. (2013). Metamaterial Huygens' Surfaces: Tailoring Wave Fronts with Reflectionless Sheets. *Phys. Rev. Lett.* 110, 197401. doi:10.1103/physrevlett.110.197401

Shi, L., Li, B., Kim, C., Kellnhofer, P., and Matusik, W. (2021). Towards Real-Time Photorealistic 3D Holography with Deep Neural Networks. *Nature* 591, 234–239. doi:10.1038/s41586-020-03152-0

Tricoles, G. (1987). Computer Generated Holograms: an Historical Review. *Appl. Opt.* 26, 4351–4357. doi:10.1364/ao.26.004351

Wang, L., Kruk, S., Tang, H., Li, T., Kravchenko, I., Neshev, D. N., et al. (2016). Grayscale Transparent Metasurface Holograms. *Optica* 3, 1504–1505. doi:10.1364/optica.3.001504

Wang, Q., Zhang, X., Xu, Y., Gu, J., Li, Y., Tian, Z., et al. (2016). Broadband Metasurface Holograms: toward Complete Phase and Amplitude Engineering. *Sci. Rep.* 6, 32867. doi:10.1038/srep32867

Wu, N., Zhang, Y., Ma, H., Chen, H., and Qian, H. (2021). Tunable High-Q Plasmonic Metasurface with Multiple Surface Lattice Resonances (Invited). *Prog. Electromagn. Res.* 172, 23–32. doi:10.2528/pier21112006

Xi, S., Chen, H., Wu, B.-I., and Kong, J. A. (2009). One-directional Perfect Cloak Created with Homogeneous Material. *IEEE Microw. Wirel. Compon. Lett.* 19, 131–133. doi:10.1109/lmwc.2009.2013677

Xu, S., Cheng, X., Xi, S., Zhang, R., Moser, H. O., Shen, Z., et al. (2012). Experimental Demonstration of a Free-Space Cylindrical Cloak without Superluminal Propagation. *Phys. Rev. Lett.* 109, 223903. doi:10.1103/physrevlett.109.223903

Xu, K., Snyman, L. W., and Aharoni, H. (2017). Si Light-Emitting Device in Integrated Photonic CMOS ICs. *Opt. Mater.* 69, 274–282. doi:10.1016/j.optmat.2017.03.055

Yan, T., Ma, Q., Sun, S., Xiao, Q., Shahid, I., Gao, X., et al. (2021). Polarization Multiplexing Hologram Realized by Anisotropic Digital Metasurface. *Adv. Theory Simul.* 4, 2100046. doi:10.1002/adts.202100046

Yang, Y., Jing, L., Zheng, B., Hao, R., Yin, W., Li, E., et al. (2016). Full-polarization 3D Metasurface Cloak with Preserved Amplitude and Phase. *Adv. Mat.* 28, 6866–6871. doi:10.1002/adma.201600625

Zhang, X., Jin, J., Wang, Y., Pu, M., Li, X., Zhao, Z., et al. (2016). Metasurface-based Broadband Hologram with High Tolerance to Fabrication Errors. *Sci. Rep.* 6, 19856. doi:10.1038/srep19856

Zhao, Z., Cheng, Q., Chen, J., Qi, M. Q., and Jiang, W. X. (2013). Tunable Metamaterial Absorber Using Varactor Diodes. *New J. Phys.* 15, 043049. doi:10.1088/1367-2630/15/4/043049

Conflict of Interest: The authors declare that the research was conducted in the absence of any commercial or financial relationships that could be construed as a potential conflict of interest.